

Received March 2, 2019, accepted March 25, 2019, date of publication March 28, 2019, date of current version April 12, 2019.

Digital Object Identifier 10.1109/ACCESS.2019.2907983

Variable Frequency Constant Current Control Method for Switched-Capacitor Converter Based Automotive LED Driver

LEI YANG¹, (Member, IEEE), WENQIAN YU, (Student Member, IEEE),
AND JIAXIANG ZHANG, (Student Member, IEEE)

School of Automation and Information Engineering, Xi'an University of Technology, Xi'an 710048, China

Corresponding author: Lei Yang (yanglei0930@gmail.com)

This work was supported in part by the China Postdoctoral Science Foundation under Grant 2018M643700, in part by the Scientific Research Project of Education Department of Shaanxi Province under Grant 18JS080, and in part by the Postdoctoral Research Grant Project of Shaanxi Province, China.

ABSTRACT A variable-frequency constant-current control (VFCCC) method with the constant t_{ON} -time is proposed in this paper for a switched-capacitor (SC) converter-based automotive LED driver. This control method is based on the one-cycle control method. The stable load current regulation could be achieved with the simple analog topology. The variable load current is conveniently set by changing the reference value. In order to reduce the current spikes, the SC topology presented in this paper introduces an inductor in the charge loop. To verify the performance of the proposed control method, a 36-W SC converter is constructed. The VFCCC-controlled SC converter is tested under different operation conditions with the different input voltages and variable constant t_{ON} -time. The experimental and simulated results show that with the proposed control method, the external disturbance could be rejected with the fast-dynamical response speed and robust performance. With the SC converter, the high-power density could be realized for the automotive LED driver. The VFCCC control method is suited for the different topologies of SC converters. It could facilitate the SC applications for the automotive LED driver.

INDEX TERMS Variable frequency constant current control (VFCCC) method, one-cycle control, switched-capacitor (SC) converter, automotive LED driver.

I. INTRODUCTION

LED drivers demand high performance with increasing functionalities [1]–[4]. LEDs provide the advantages such as high luminous efficiency and long lifetime [1], [5]–[8]. The performance of LEDs mainly depends on a driver. A LED driver should be an attractive and low-cost solution while accomplishing a high performance [9]–[15].

LED bulbs could provide the same amount of light as traditional incandescent car bulbs with less energy [16]. For LED lamps, the advantages such as the cooler temps, longer lifespan, and greater stylistic freedom can be transferred to be the longer road range on a single charge for the electric vehicles. As the advantages of the LEDs, they have been widely used for the environmental-friendly applications such as electric vehicles [17]–[20]. In the applications of LED

lamps for electric vehicles, the power source is the batteries [21]. As a result, the input current and load current ripple, which will influence the lifespan of the batteries, should be small enough.

In order to improve the performance of LED drivers, SC converter has been explored. Switched-capacitor (SC) converter is used for the different low power and high-power applications with the high-power density, small size, and light weight [22]–[26]. The SC converters are only composed of switches and capacitors. The energy transfer is achieved by adjusting the charging and discharging periods of the switched capacitors. The resonant switched capacitor converter has been invented to reduce the pulsating current in the charge loop and discharge loop of SC converter to realize the high energy efficiency and the low EMI noise [27]–[31].

A dimmable resonant-switched capacitor LED driver with variable inductor control is shown in [29]–[30]. It provides a simple and cost-effective solution for the LED driver with

The associate editor coordinating the review of this manuscript and approving it for publication was Yijie Wang.

the simple topology. However, it is not easy to achieve the variable inductance to control the mean value of the LED lamp current. The research study presented in [32] provides a frequency modulated SC converter to drive LEDs. The average current proportionally depends on the difference between the supply voltage and the forward voltage of LEDs. The LED array will be affected by the variable forward voltage of LEDs. Besides, the forward voltage also depends on the LED junction temperature, making this proposal inadequate for the open-loop operation. Paper [33] provides a SC converter driver with the 24V DC source. Unlike the conventional SC converters, the proposed SC converter in [33] adopts a small additional magnetic component to make the power delivered to the LEDs does not depend on the forward voltage. It improves the efficiency of SC converter. Paper [34] presents a LED driver based on the three-phase resonant SC converter. The low ripple current and the small percent flicker could be accomplished by adopting the proposed three-phase structure. Variable LED dimming could be obtained by changing the switching frequency.

When it comes to the automotive LED driver, there are different kinds of topologies are provided. A topology-transition control for automotive LED driver is proposed in [17]. It could provide the fast-current regulation in the wide-input voltage range. The maximum energy efficiency is realized around the voltage gain ratio 1. A high-frequency, digitally controlled high-brightness LED driver for automotive applications with fast dimming capabilities was proposed as shown in [19]. The power converter is based on the magnetically coupled Cuk topology and employs a single, off the-shelf SMT mutual inductor. In combination with a dedicated duty cycle feedforward technique, the load current is regulated. Paper [35] presents a PWM-based LED driver that features low EMI noise and high reliability. The buck-based LED driver is regulated by the average current control method and the good current balance and small current ripple is obtained. However, with the inductor-based converter, the power density of LED driver is not high enough. The conventional PWM control scheme (i.e., peak current control) suffers from two issues [35]. One is the the average output current is imprecise. The other is subharmonic oscillation when the duty cycle is larger than 0.5. What's more, the dynamic response speed is not high enough for the linear control method.

A constant on time variable frequency one-cycle control (CVFOCC) method is proposed in [36] for SC converters. It is designed to accomplish the continuous variable conversion ratio and fast-dynamical response speed to reject the external disturbance. This control method is based on the dynamic capacitor-ampere second balance modeling method [37] and the one-cycle control method [38]. A proper regulation could be obtained by controlling the related "off time" of a transistor with the constant "on time" which is less than the time constant τ of the charge loop. Based on the dynamic capacitor ampere-second balance principle and the one cycle control method, the robust output voltage regulation is achieved with the fast-dynamic response speed as shown in [36].

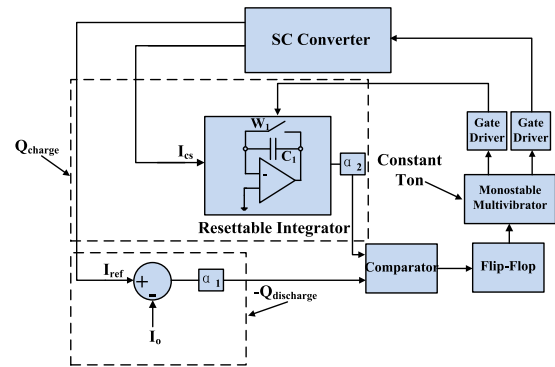


FIGURE 1. Closed feed-back loop of proposed controller.

For the future electric vehicles, the LED drivers should provide the good features: high power density, cost-effective, simple topology, and good regulation with the fast-dynamic response speed.

A topology of a resonant SC converter shown in [33] is adopted in this paper to verify the proposed constant current control method. An inductor which is injected into the charge loop to reduce the pulsating current which occurring in the general SC converter. However, the SC converter is controlled by the open-loop control method in [33]. It cannot reject the external disturbance. The load current regulation is not good enough. The maximum efficiency is less than 85%. In this paper, based on the research study in [36] and [38], the authors propose a nonlinear constant on time variable frequency constant current control (VFCCC) method for the SC converter-based automotive LED driver. The closed feedback loop of proposed controller is shown as Fig.1. Compared with the research work in [36], the constant current regulation of SC converter is achieved in this paper. The output current of SC converter could be kept stable by adjusting the switching frequency with the constant on time. In one switching cycle, the charge of capacitor and discharge of capacitor is kept balance by integrating the charging current of capacitor in the charging period and integrating the discharging current of capacitor in the discharging period. The PI control method is the linear control method. However, the charging and discharging of SC converter is a nonlinear operation. Compared with the PI control method, the nonlinear VFCCC control method will provides more stable performance with the fast-dynamical response speed.

With the VFCCC method, the SC converter provides good performance. What's more, the dimming of LEDs could be rearranged by just changing the reference current. In order to build the control topology, the charge balance principle is adopted in this paper. The primary objective of this paper is to explore the VFCCC method for SC converter-based automotive LED driver and to provide systematic analysis to address the regulation issue for the electric vehicles. The rest of paper is organized as follows: the topology and the operation principle of SC converter-based automotive LED driver is investigated in section II. The modeling and operation analysis for the proposed control method is provided

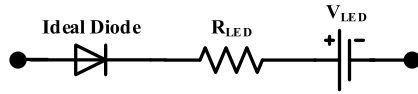


FIGURE 2. Equivalent electrical model of LEDs.

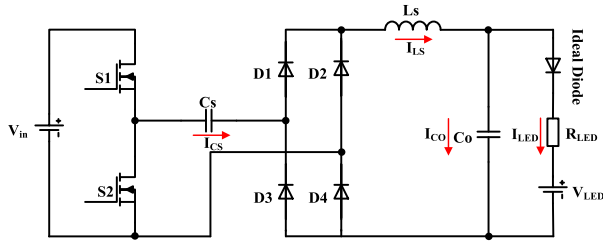


FIGURE 3. Topology of SC converter based automotive LED driver.

in section III. Section IV shows the experimental verification. In section V, the conclusions and discussions are drawn.

II. SC CONVERTER TOPOLOGY ANALYSIS

Fig.2 shows a simplified LED model. It is composed of the intrinsic series resistance, the ideal diode, and the power source of LED. The LED intrinsic series resistance is due to the current diffusion in the semiconductor and the device is designed for the low value to minimize losses.

The SC converter-based automotive LED driver used in this paper is shown in Fig.3. This SC converter works in the discontinuous conduction mode (DCM). As shown in Fig.4, there are six equivalent operation states. The operation timing waveforms are presented in Fig.5. An inductor is injected into the topology to make the power which delivered to the LED do not depend on the forward voltage. This issue can be achieved by increasing the on time of SC converter which could reduce the peak currents through the circuit. The capacitor C_s is charged and discharged in one switching cycle. The energy stored in the capacitor C_s is transferred to the filter capacitor C_o and the power LED.

The following assumptions are made to facilitate the modeling calculation: (a) S_1 and S_2 are identical with the same internal resistance ($R_{s1} = R_{s2} = R_q$). (b) The capacitance of C_o is large enough to ensure the voltage characteristic imposed by LEDs. (c) When switch S_1 is turned on, switch S_2 must be turned off and vice versa. (d) Diodes D_1, D_2, D_3 and D_4 are identical with the same internal resistance ($R_{d1} = R_{d2} = R_{d3} = R_{d4} = R_d$). The operation of SC converter presented in this paper could be divided into six states as shown in Fig.4 and Fig.5.

Fig.3(a) shows the State 1 ($t_0 - t_2$). When switch S_1 is ON while switch S_2 is OFF, the capacitor C_s , inductor L_s , and filter capacitor C_o are charged by power source. During the period of State 1, the maximum voltage across capacitor C_s is V_{in} . At time t_1 , the maximum current flows through capacitor C_s . The current through capacitor C_s reduces to zero at time instant t_2 .

Fig3(b) shows the State 2 ($t_2 - t_3$). The switch S_2 is kept OFF and there is no current flowing through switch S_1 ,

diodes D_1, D_2, D_3 and D_4 are all ON, the inductor L_s delivers its stored energy to capacitor C_o and load power LEDs. At time instant t_3 , the current of inductor L_s reaches zero.

Fig.3(c) shows the State 3 ($t_3 - t_4$), the capacitor C_o transfers its stored energy to the load power LEDs. The half energy which provided by the power source is stored in the capacitor C_s at the time point t_3 . The other half energy is delivered to the capacitor C_o and the load power LEDs.

Fig.3(d) shows the State 4 ($t_4 - t_6$), when switch S_2 is ON while switch S_1 is OFF, capacitor C_s delivers its stored energy to inductor L_s , the load power LEDs, and capacitor C_o . The original voltage across capacitor C_s is equal to V_{in} . At time point t_5 , the maximum current of capacitor C_s is achieved. The voltage across capacitor C_s reduces to zero at time t_6 .

Fig.3(e) shows the State 5 ($t_6 - t_7$). The switch S_1 is kept OFF and there is no current flowing through switch S_2 , diodes D_1, D_2, D_3 and D_4 are all ON. Inductor L_s transfers its stored energy to the capacitor C_o and load power LED. This state is similar to State 2.

Fig.3(f) shows the State 6 ($t_7 - t_8$). Capacitor C_o transfers its stored energy to the load power LEDs. This state is similar to State 3.

III. OPERATION AND CALCULATION

Paper [37] presents a capacitor ampere-second balance transient (CASBTC) modeling method. The work in [37] is based on the instantaneous charge balance calculation in the charging period and discharging period to realize the stable voltage regulation. However, in this paper, in order to achieve the constant current regulation, the one cycle charge balance of capacitor is directly built by introducing the instantaneous charging current of capacitor and discharging current of capacitor to the key modeling equation. As a result, the theory and the modeling method in this paper is different from the work in [37]. This modeling method is conducted based on the “on time” and “off time” or “one switching cycle time” of a transistor instead of the duty-cycle. It yields accurate transient and steady-state prediction of SC converters in the wide operation range.

A. OPERATION ANALYSIS FOR THE PROPOSED METHOD

The operation of the SC converter is based on the charge balance of capacitor C_s . The charge in the charging period of C_s is equal to the discharge in the discharging period of C_s . In this paper, the charging time for C_s is kept constant (T_{on}). The load current regulation could be achieved by changing the discharging time of C_s (T_{off}).

In the following calculation, the resonant frequency of the circuit can be defined as $\omega_o = \sqrt{\frac{1}{L_s \times C_s}}$.

In State 1 ($t_0 - t_2$), according to KVL principle, the instantaneous voltage through the capacitor C_s can be written as:

$$V_{cs}(t) = -(V_{in} - V_o) \cos(\omega_o t_2) + (V_{in} - V_o) \quad (1)$$

where V_{in} is the input voltage, and V_o is the output voltage.

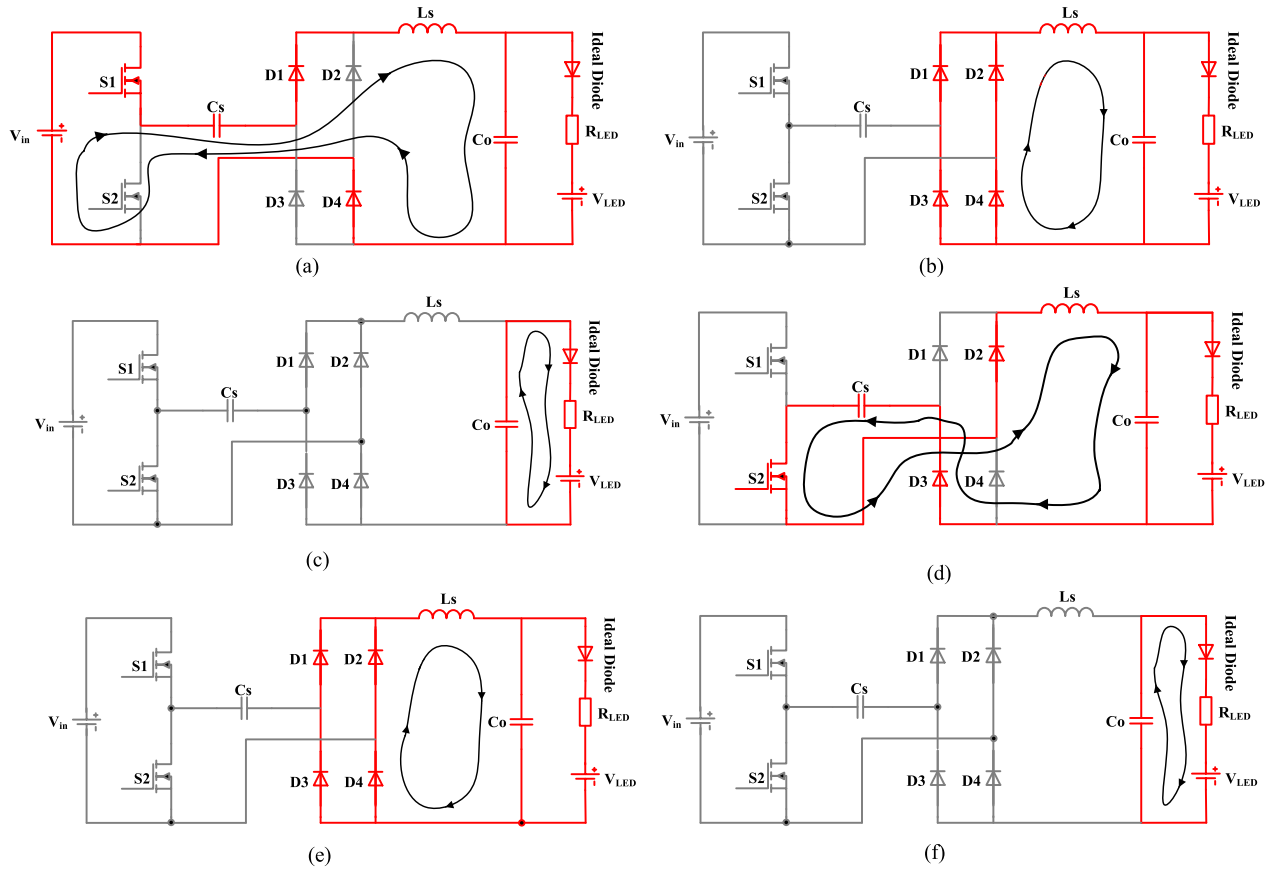


FIGURE 4. Equivalent operation states of SC converter based automotive LED driver. (a) State 1. (b) State 2. (c) State 3. (d) State 4. (e) State 5. (f) State 6.

The voltage of the inductor L_s can be derived as:

$$L_s \frac{di_{L_s}}{dt} = u_{L_s} \quad (2)$$

The inductor current i_{L_s} can be expressed as:

$$i_{L_s}(t) = \sqrt{\frac{C_s}{L_s}} (V_{in} - V_o) \sin(\omega_o t) \quad (3)$$

The voltage of the capacitor C_s is equal to the input voltage V_{in} at time point t_2 , it can be written as:

$$V_{cs(t_2)} = V_{in} \quad (4)$$

The time t_2 could be derived by considering the equation (4). It can be written as:

$$t_2 = \sqrt{L_s \times C_s} \arccos\left(\frac{V_o}{V_o - V_{in}}\right) \quad (5)$$

When the capacitor C_s delivers its energy (at $t = t_4$), the energy of capacitor C_s can be expressed as:

$$E_{C_s}(t_4) = \frac{1}{2} C_s \times V_{in}^2 \quad (6)$$

In State 4-State 6 (which is the second half of one switching cycle), the energy stored in the capacitor C_s is transferred to the subsequent LED lamps group and the filter

capacitor C_o . Therefore, the average power transferred to the output represented by P_o , which corresponds to the very power of the LED array. Based on the expression (6), the average output power P_o could be obtained as:

$$P_o = 2E_{C_s}(t_4) \times f_s \times \eta = C_s \times V_{in}^2 \times f_s \times \eta \quad (7)$$

where η is the efficiency of SC converter and f_s is the switching frequency.

Equation (7) represents the power of the LED lamp group. It could also be written as:

$$P_o = V_o \times I_{AVG} \quad (8)$$

where I_{AVG} is the average load current of the power LED.

The output voltage of the LED lamp can be derived as:

$$V_o = V_{LED} + R_{LED} \times I_{AVG} \quad (9)$$

where V_{LED} is the forward voltage of the power LED, and R_{LED} is the LED intrinsic series resistance.

Substituting (8) and (9) into (7), C_s could be written as:

$$C_s = \frac{V_o \times I_{AVG}}{V_{in}^2 \times f_s \times \eta} \quad (10)$$

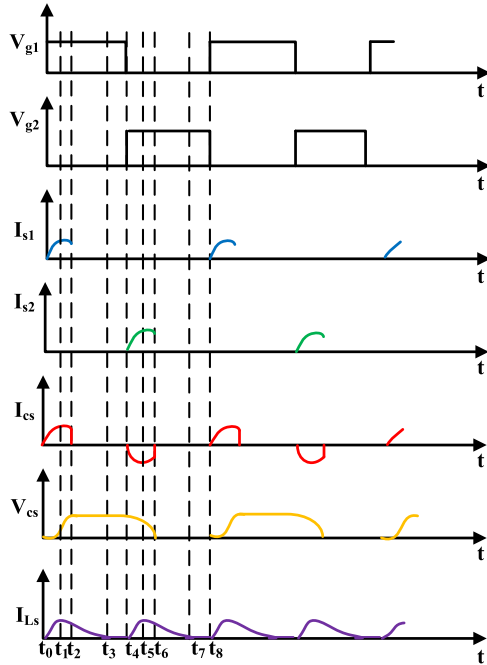


FIGURE 5. Timing waveforms of SC converter based automotive LED driver.

The 10% current ripple of ΔI_{LED} is set. As a result, C_o could be expressed as:

$$C_o = \frac{2}{3\Delta I_{LED} (2\pi f_s) R_{LED}} \quad (11)$$

There are two operation states for capacitor C_s : one is the charge state, and the other is the discharge state. The resistance of the charge loop and discharge loop could be respectively written as:

$$R_{ch} = R_{s1} + R_{cs} + R_{d1} + R_{Ls} + R_{d4} + \frac{R_{co} \times R_{Led}}{R_{co} + R_{Led}} \quad (12)$$

$$R_{dis} = R_{s2} + R_{cs} + R_{d2} + R_{Ls} + R_{d3} + \frac{R_{co} \times R_{Led}}{R_{co} + R_{Led}} \quad (13)$$

where R_{cs} , R_{co} , and R_{Ls} are the equivalent series resistance (ESR) of capacitor C_s , capacitor C_o and inductor L_s . R_{s1} and R_{s2} are the “on resistance” of switches S_1 and S_2 , respectively. $R_{d1} \sim R_{d4}$ are the “on resistance” of diodes $d_1 \sim d_4$.

In the charging period, switch S_1 is ON while switch S_2 is OFF. The power source transfers its energy to capacitor C_s during the constant on-time (T_{on}) period. The instantaneous charging current of capacitor C_s is expressed as:

$$I_{ch}(t) = \frac{V_{in} - V_{cs}(t) - V_{Ls}(t) - V_o}{R_{ch}} = C_s \frac{dV_{cs(charging)}}{dt} \quad (14)$$

where $V_{cs}(t)$ and $V_{Ls}(t)$ are respectively the instantaneous voltage of C_s and L_s .

In the discharging period, switch S_2 is ON, switch S_1 is OFF, capacitor C_s delivers its stored energy to the load in

the T_{off} time period. The instantaneous discharging current of capacitor C_s is written as:

$$-I_{dis}(t) = \frac{V_{cs}(t) - V_{Ls}(t) - V_o}{R_{dis}} = -C_s \frac{dV_{cs(discharging)}}{dt} \quad (15)$$

According to the charge balance principle of capacitor C_s , the charge (Q_{charge}) of capacitor C_s during the charging period is equal to the negative discharge ($Q_{discharge}$) of capacitor C_s during the discharging period. It abides by the following equation:

$$Q_{charge} + Q_{discharge} = I_{ch}(t) T_{on} + I_{dis}(t) T_{off} \quad (16)$$

Based on the equations (14) and (15), the charge Q_{charge} of capacitor C_s during the charging process of capacitor C_s can be expressed as:

$$Q_{charge} = \int_0^{T_{on}} I_{ch}(t) dt = \int_0^{T_{on}} \frac{V_{in} - V_{cs}(t) - V_{Ls}(t) - V_o}{R_{ch}} dt \quad (17)$$

What’s more, the discharge $Q_{discharge}$ of capacitor C_s during the discharging process can be written as:

$$-Q_{discharge} = \int_{T_{on}}^{T_s} [-I_{dis}(t)] dt = \left(\frac{V_{cs}(t) - V_{Ls}(t) - V_o}{R_{dis}} \right) T_{off} \quad (18)$$

Submitting equations (17) and (18) into (16) and letting $a_1 = \frac{1}{R_{ch}}$ and $a_2 = \frac{1}{R_{dis}}$, the one switching cycle charge balance of SC converter could be written as:

$$a_1 \int_0^{T_{on}} (V_{in} - V_{cs}(t) - V_{Ls}(t) - V_o) dt = a_2 (V_{cs}(t) - V_{Ls}(t) - V_o) T_{off} \quad (19)$$

As shown in equations (17)-(19), the real-time state of charging current of capacitor C_s and the real-time state of the discharging current of capacitor C_s are included in the dynamic ampere-second balance model. As a result, the disturbance in the input voltage and the perturbation in the load current could be quickly rejected.

In the charging period, the instantaneous charging current of charge loop $I_{ch}(t)$ is equal to the instantaneous current of capacitor C_s . It could be expressed as:

$$I_{ch}(t) = I_{cs}(t) = \frac{V_{in} - V_{cs}(t) - V_{Ls}(t) - V_o}{R_{ch}} \quad (20)$$

Setting the reference current as:

$$I_{ref} = \left(\frac{\overline{V_{CS}(t)} - \overline{V_{LS}(t)}}{R_{dis}} \right) \quad (21)$$

What’s more, the load current could be written as:

$$I_o = \frac{V_o}{R_{dis}} \quad (22)$$

The average discharging current, the reference current and the load current have a relationship as:

$$\overline{I_{dis}(t)} = I_{ref} - I_o = \frac{\overline{V_{Cs}(t)} - \overline{V_{Ls}(t)} - V_o}{R_{dis}} \quad (23)$$

where $I_{dis}(t)$ is the instantaneous discharging current of capacitor C_s .

Considering equations (22) and (23), the one switching cycle charge balance equation (19) of SC converter could be rearranged as:

$$a_1 \int_0^{T_{on}} I_{Cs}(t) dt = a_2 (I_{ref} - I_o) T_{off} \quad (24)$$

The left part of equation (24) is the one cycle charge of capacitor C_s . The right part of equation (24) is the one cycle discharge of capacitor C_s .

It is worthwhile mentioning that the equation (24) is the key equation for the proposed VFCCC method in this paper. The proposed VFCCC controller is constructed based on equation (24).

During the time period $(0-T_{on})$ of switch S_1 , the following equations could be derived as:

$$V_{in} = V_{Cs} + L_s \frac{di_{Ls}}{dt} + V_o \quad (25)$$

$$i_{Ls} = i_{Cs} = C_s \frac{dV_{Cs}}{dt} \quad (26)$$

$$V_{Cs}(0) = V_{Csmin} \quad (27)$$

Based on equations (25)-(27), the instantaneous voltage of capacitor C_s could be derived as:

$$V_{Cs}(t) = (V_{Csmin} - V_{in} + V_o) \cos \frac{1}{\sqrt{L_s C_s}} t + C_s \sin \frac{1}{\sqrt{L_s C_s}} t + V_{in} - V_o \quad (28)$$

As $\omega_o = \sqrt{\frac{1}{L_s \times C_s}}$, the equation (28) could be rearranged as:

$$V_{Cs}(t) = (V_{Csmin} - V_{in} + V_o) \cos(\omega_o t) + V_o \sin(\omega_o t) + V_{in} - V_o \quad (29)$$

When $\omega_o t = \frac{\pi}{2}$, the maximum voltage of capacitor C_s could be written as:

$$V_{Csmax} = V_{Cs}(t) T_{on} = V_{in} \quad (30)$$

When switch S_2 is turned on while switch S_1 is turned off, the energy stored in the capacitor C_s will be transferred to the filter capacitor C_o and the load power LEDs array, the charge balance of capacitor C_s can be derived as:

$$C_s (V_{Csmax} - V_{Csmin}) = \frac{(T_s - T_{on}) V_o}{R_{dis}} \quad (31)$$

The maximum voltage of capacitor C_s in one switching cycle could be derived as:

$$V_{Csmax} = \int_0^{T_{on}} V_{Cs}(t) dt \quad (32)$$

Considering equation (31), the equation (32) could be rewritten as:

$$V_{Csmax} = V_{Csmin} - V_{in} + 2V_o + (V_{in} - V_o) T_{on} \quad (33)$$

Submitting (33) into (31), the voltage gain of SC converter-based automotive LED driver could be given as:

$$\frac{V_o}{V_{in} - V_d} = \frac{2}{1 + \left(1 + \frac{T_s}{2T_{on}}\right) \left(\frac{R_{dis}}{R_L}\right)} \quad (34)$$

where V_d is the voltage of a diode.

It can be seen from equation (34), the voltage gain ratio of SC converter is regulated by control parameter $\frac{T_{on}}{T_s}$. At the same time, the gain ratio will be affected by discharging loop resistance R_{dis} and the load resistance R_L .

When the SC converter works in the DCM, the inductor of SC converter should satisfy the following equation:

$$L_s < \frac{1}{(2\pi \times f_s)^2 \times C_s} \quad (35)$$

The switching frequency of SC converter should abide the operation range as:

$$0 < f_s < \frac{1}{2\pi} \sqrt{\frac{1}{L_s \times C_s}} \quad (36)$$

The SC converter will be properly controlled by the proposed control technique with the key control equations (19) and (24). It can be observed from equations (19) and (24), based on the dynamic ampere-second balance modeling method, the input voltage, instantaneous voltage of capacitor C_s , instantaneous voltage of inductor L_s , average voltage of capacitor C_s , output voltage of SC converter, current of capacitor, reference current, load current, on time of the transistor, and off time of the transistor are all included in this model equation. It indicates that the closed-loop system will instantaneously reject the disturbances in power source and load by adjusting the switching frequency with the constant on time as shown in [36]–[37]. The dynamic ampere-second balance method in this paper is a dynamic modeling method. As a result, the instantaneous states of different parameters could be mirrored in this modeling method.

With the resettable integrator which will be presented in the control circuit, the control decision of current switching cycle is independent of the history states.

B. CONTROLLER TOPOLOGY

The controller circuit adopted in this paper is shown as Fig.6. The timing waveforms for this configuration is presented in Fig.7. According to the key control equation (24) and the OCC controller, the proposed VFCCC controller is constructed. The controller circuit for the VFCCC method proposed in this paper and the controller in [36] is totally different with each other. Compared with the CVFOCC controller as shown in [36], the charge current of the capacitor C_s is directly injected into resettable integrator and the integration represents the charge of the capacitor C_s . On the other

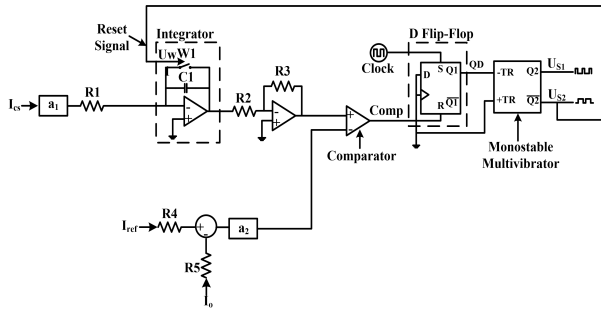


FIGURE 6. Control topology for SC converter based automotive LED driver.

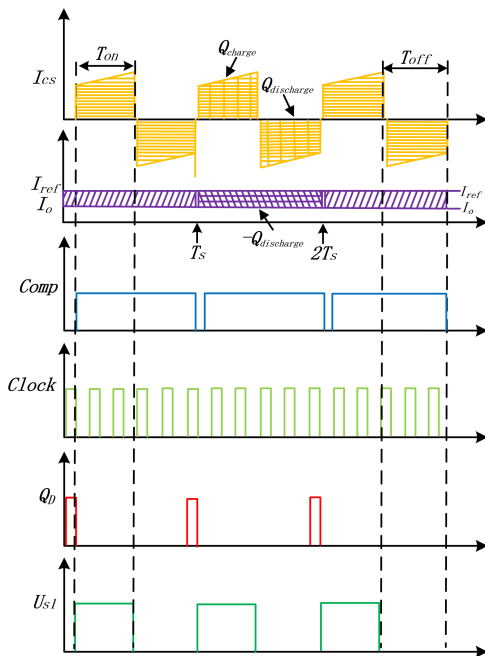


FIGURE 7. Timing waveforms of proposed controller.

hand, the load current and the reference current are added to the negative part of comparator and the summation represents the discharge of the capacitor C_s . The proposed controller is composed of a comparator, a resettable integrator, a D flipflop, a monostable multivibrator (which can produce the constant on time PWM signal), and some other passive components. The two current sensors (Hall Effect-Based Linear Current Sensor IC, ACS714ELCTR-20A-T) for testing the instantaneous current of the capacitor C_s and instantaneous current of the load current should be injected into the SC circuit for the control circuit.

As the operation of switches S_1 and S_2 are complementarily with each other, switch S_2 must be turned off when switch S_1 is turned on, and vice versa. The control signals for switches S_1 and S_2 have the relationship $U_{s1} = \overline{U_{s2}}$. As the relationship of U_{s1} and U_{s2} , the only controlled signal is U_{s1} in this paper.

It can be seen from Fig.6 and Fig.7, when the clock signal arrives, the D flip-flop in Fig.6 is set high state ($Q1 = 1, \overline{Q1} = 0$). The constant pulse width square signal U_{s1} ($Q2 = U_{s1} = 1, \overline{Q2} = U_{s2} = U_{W1} = 0$) (which represents the

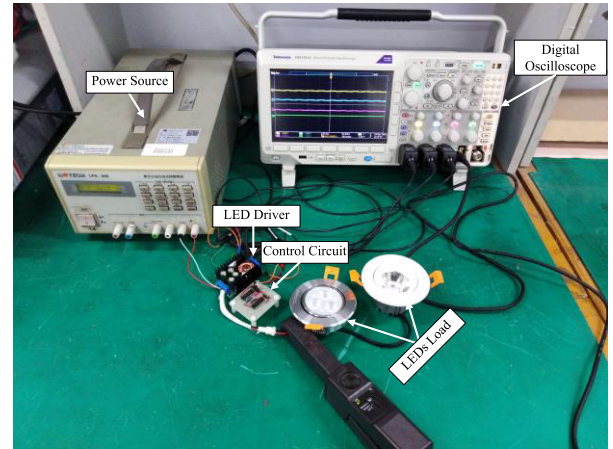


FIGURE 8. Experimental setup for the proposed control method.

constant T_{on} time period) will be generated by monostable multivibrator in Fig.6 at the time point of the falling edge of Q_D signal of D flip-flop. The control PWM signal U_{s1} will turn on the switch S_1 in Fig.3. While, the control PWM signal U_{W1} will maintain the resettable switch W_1 (the resettable switch of the integrator) off in Fig.6. As switch S_2 shares the same control PWM signal of switch W_1 of the resettable integrator, the switch S_2 in Fig.3 will be kept off during the T_{on} time period. For T_{on} time period, the charging current of capacitor C_s [$I_{cs}(t)$] is continually integrated by the resettable integrator. When T_{on} is over, the monostable multivibrator will be reset low state ($Q2 = U_{s1} = 0, \overline{Q2} = U_{s2} = U_{W1} = 1$). The resettable switch W_1 is ON. As a result, the value of the integration in Fig.6 will be set zero at this time point. The switch S_2 in Fig.3 is turned on by the control signal U_{s2} . During the T_{off} time period, if the negative discharge of capacitor C_s [$-Q_{discharge} = I_{dis}(t)T_{off} = a_2(I_{ref} - I_o)T_{off}$] is equal to the charge amount of capacitor C_s (Q_{charge}), the state of comparator in Fig.6 will be changed from high to low. In one cycle, the charge balance of capacitor C_s is reached. The operation will repeat in the new switching cycle. With the proposed control method, the external perturbation will be rejected by adjusting the T_{off} time period or the switching frequency.

Fig.7 shows the timing waveforms of the proposed controller. It can be seen from Fig.7 that, the falling edge of Q_D signal of D flip-flop will trigger the monostable multivibrator which will generate a constant pulse width square signal U_{s1} ($U_{s1} = 1, U_{W1} = U_{s2} = 0$) (constant T_{on} time period) for switch S_1 in Fig.3. At the the same time point, the resettable switch W_1 will be turned off. The charge of capacitor C_s will be produced by integrating the charging current of C_s [$I_{cs}(t)$] during T_{on} time period. As shown in Fig.7, the state of comparator (Comp) in Fig.6 will change from high to low when the negative discharge of capacitor C_s ($-Q_{discharge}$) is equal to the the charge of C_s (Q_{charge}). This time point is the end of T_{off} time period. The one cycle charge balance of capacitor C_s is achieved. If the D flip-flop outputs another falling edge of Q_D signal, the

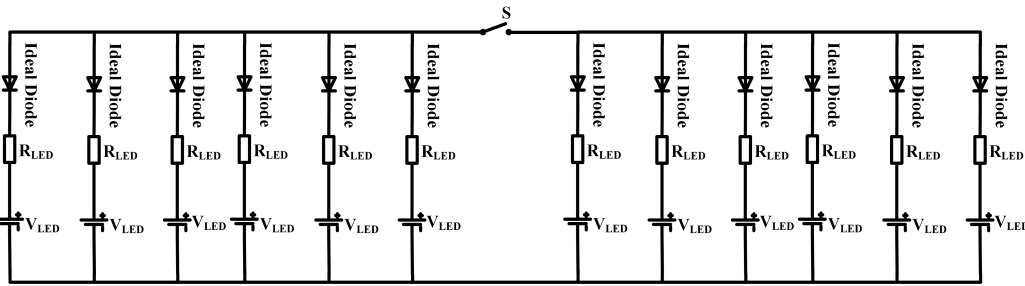


FIGURE 9. Connection type of LEDs load.

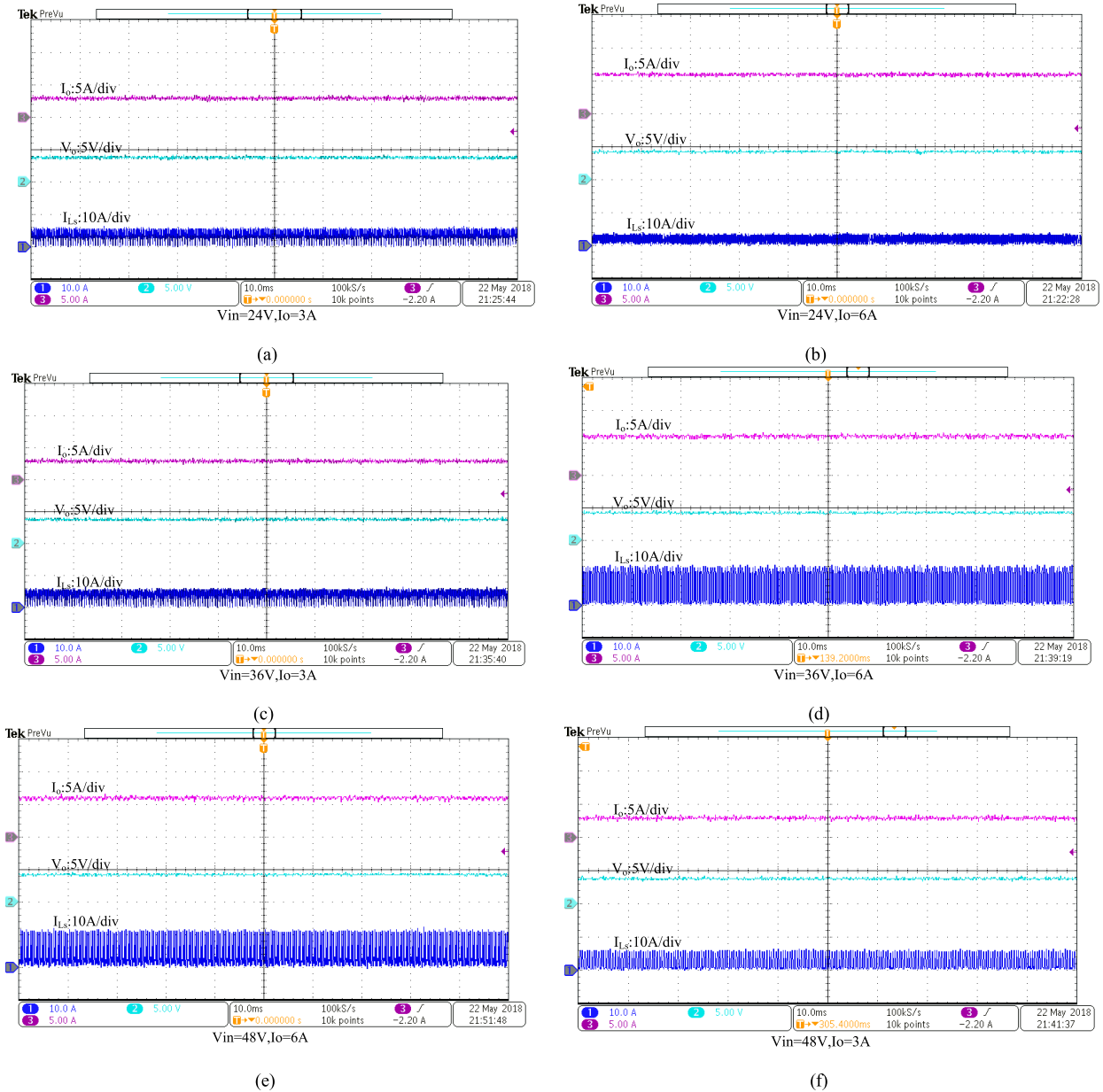


FIGURE 10. Steady-state experimental waveforms of proposed control method controlled SC converter.

monostable multivibrator will generates a new control signal U_{s1} ($U_{s1} = 1, U_{W1} = U_{S2} = 0$) (constant T_{on} time period) for switch S_1 in Fig.3. The resettable switch W_1 will be turned

off and the resettable integrator in Fig.6 will work again for the new switching cycle. It can be seen from Fig.7 that, the control signal U_{s1} for switch S_1 in Fig.3 has constant

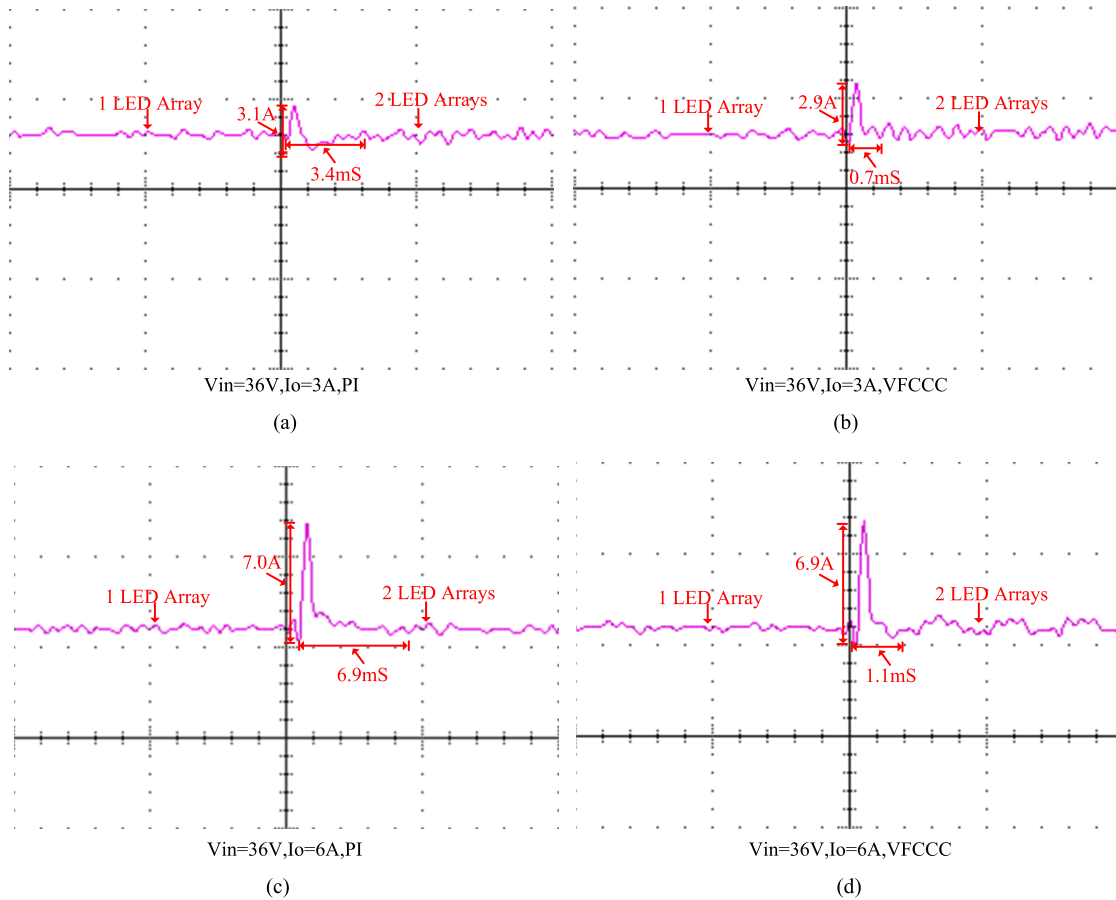


FIGURE 11. Comparison of dynamic response speed between the PI control method and the VFCCC method with the adjustable loads.

“on time” T_{on} . However, the switch S_1 will have a variable T_{off} to adjust switching frequency and to reject the external disturbance. A SC converter could be regulated unless that the “on time” of a transistor is less than constant $\tau = \frac{1}{RLC}$ of charge loop of RLC circuit. In this paper, the operation range of a SC converter will be widely extended by setting the constant T_{on} of switch S_1 much less than the time constant $\tau = \frac{1}{RLC}$ of RLC circuit which is composed of the inductor L_s and the capacitor C_s . By changing the T_{off} time period of switch S_1 , the regulation of SC converter could be reached.

The external perturbation could be quickly rejected by adjusting the T_{off} time period or switching frequency. As shown in Fig.7, setting the load current I_o and the reference current I_{ref} stable, if a voltage step-up function is happened in the power source, an increase will be immediately occurred in the charging current of capacitor $C_s [I_{cs}(t) = \frac{V_{in} - V_{cs}(t) - V_{Ls}(t) - V_o}{R_{ch}}]$. The monostable multivibrator will keep T_{on} of switch S_1 constant. As a result, the charge of capacitor $C_s [Q_{charge} = \int_0^{T_{on}} I_{cs}(t) dt]$ will increase correspondingly during the T_{on} time period. According to the charge balance principle of capacitor $C_s (Q_{charge} = -Q_{discharge})$, the T_{off} will increase and the corresponding switching frequency will decrease. While, if a voltage step-down function is happened

in the power source, the T_{off} will decrease and the corresponding switching frequency will increase.

As shown in Fig.7, setting the the input voltage V_{in} and load current I_o stable, the charge Q_{charge} of C_s during the T_{on} time period is maintained constant. According to the charge balance principle ($Q_{charge} = -Q_{discharge}$), if the reference current I_{ref} rises, the T_{off} will decrease and the corresponding switching frequency will increase. On the other hand, with the decreased I_{ref} , T_s will increase the corresponding switching frequency will decrease.

IV. EXPERIMENTAL VERIFICATION

In order to verify the accuracy of proposed control method and the theory analysis, a 36W SC converter is built. This SC convert works in the DCM. The input voltage range is from 24V to 48V. The load current is adjusted from 3-6A. The frequency of the clock signal for the D Flip-Flop is set 50kHz (which is less than the resonant frequency of SC converter). The two constant on time T_{on} values (5us and 10us) are adopted by setting the monostable multivibrator, respectively. The dynamic and the steady state performance of the proposed control method-controlled SC converter are both tested. The dynamic response speed is compared with the PI control method in the same operation condition.

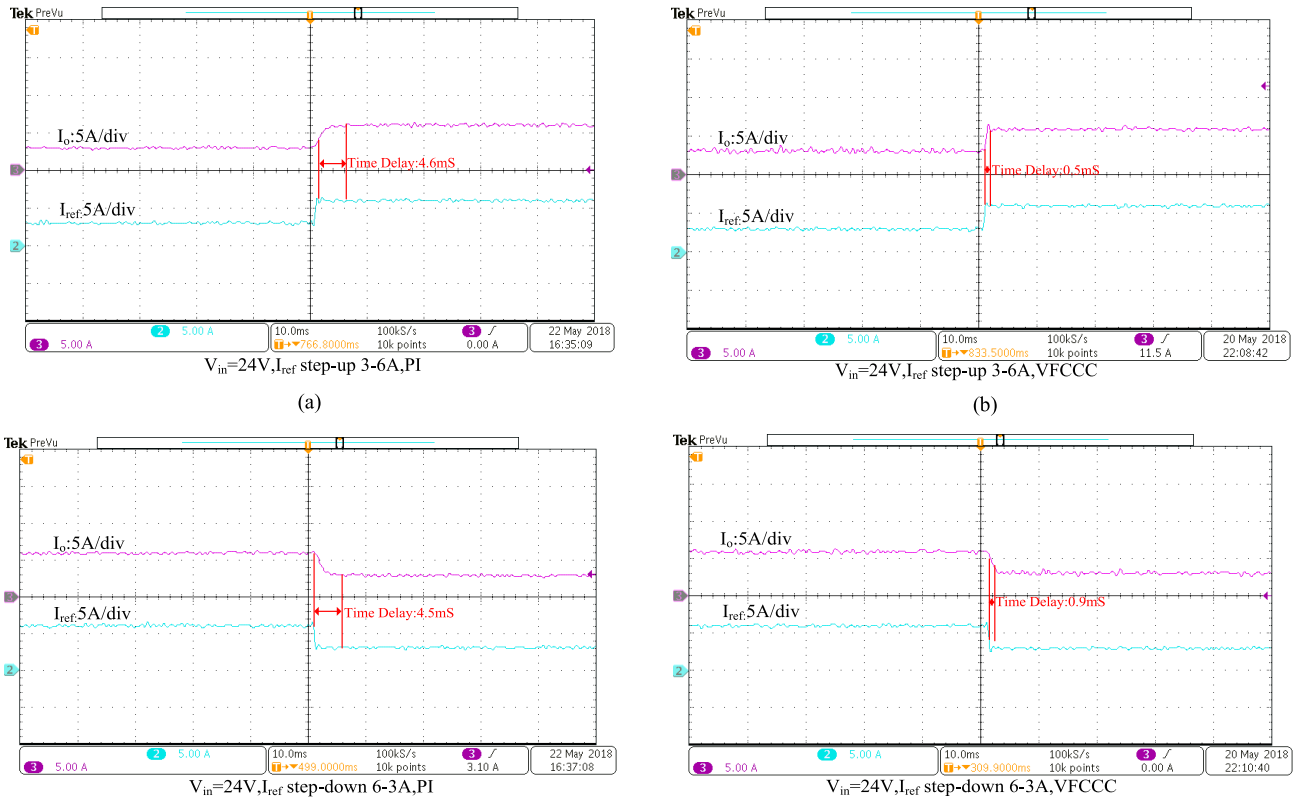


FIGURE 12. Comparison of dynamic response speed between the PI control method and the VFCCC method with the adjustable reference currents.

TABLE 1. Circuit parameters of SC converter based automotive led driver.

Circuit parameters	Value/Type
Input voltage	24-48V
Load Current	0-6A
Inductor L_s	22uH
Capacitor C_s	47nF
Clock frequency	50kHz
Switches S_1 and S_2	IRF540
Diodes D_1 - D_2	MBR40100WT
Constant on time T_{on}	5us and 10us
Current Sensor (ACS714ELCTR-20A-T)	±20A

The energy efficiency of SC converter is measured in different power levels. The detailed parameters of SC converter presented in this paper is shown in Table 1. The experimental setup is shown in Fig.8. The intrinsic resistance and the forward voltage of one LED adopted in this paper are respectively 0.9Ω and 3.15V. It adopts 6 LEDs as one LEDs array and 12 LEDs as two LEDs arrays as shown in Fig.9. The LEDs are parallel connected. The 5W,750mA LED is used in the experiment. The different load types could be changed by changing the switch S . The LED dimming could be changed by adjusting the reference current.

A. STEADY-STATE REGULATION

The steady-state experimental operating waveforms of the output voltage, load current, and the current of inductor L_s

are shown in Fig.10. The experiments are conducted under the input voltage conditions 24V,36V and 48V, and the load current conditions 3A and 6A with the constant on time 10us. It can be seen from Fig.10, the load current, the output voltage, and the current of the inductor are kept stable in the operation process. With the variable input voltage, the target load current (3A and 6A) is achieved with small current ripple. The higher input voltage, the larger input current ripple will occur. As shown in Fig.10, with the small value inductor in the SC converter presented in this paper, the continuous input current is achieved. The VFCCC controlled SC converter shows the good load and line regulation properties.

B. DYNAMIC PERFORMANCE

The dynamical property of SC converter in handling load current disturbance and the reference current perturbation is investigated for both the PI control method (switching frequency 50kHz, $K_p = 0.4$ and $K_z = 100$) and the VFCCC method (the constant on time is 5us). As shown in Fig.11, the reference current is kept stable and the external disturbance is injected into the load current (the load LEDs is switched from one array to two arrays). It can be seen from Fig.11 that, for the same load current (3A or 6A), with the proposed control method, the SC converter provides much less response time at the transient time point than the PI controlled SC converter. With the proposed controller, the worst-case transient setting time of SC converter is 1.1mS. As compared to the worst-case

TABLE 2. Comparison with prior art.

Type of LED Driver	Control Method	Efficiency (Maximum)	Power Density	Response Speed	Topology
Paper [19]	PI Control(Simple)	89.7%	Medium	Fast	Medium
Paper [30]	Variable inductor Control (Medium)	/	High	Medium	Simple
Paper [33]	Open-loop (Simple)	83%	High	Slow	Simple
Paper [35]	Average current control (Complex)	94.7%	Low	Fast	Simple
This Work	VFCCC(Medium)	97.4%	High	Fast	Simple

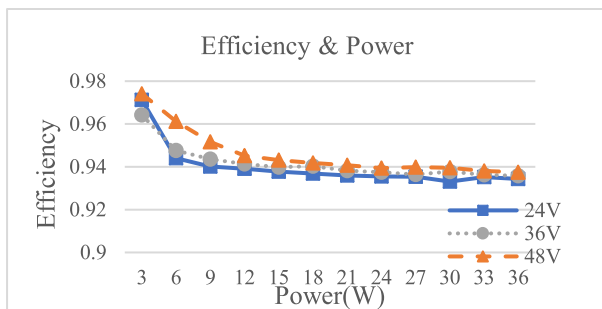


FIGURE 13. Measured efficiency with the input voltage 24V,36V,and 48V and variable output power ($T_{on} = 5\mu s$).

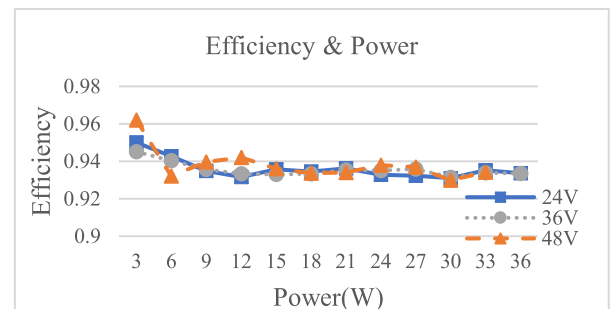


FIGURE 14. Measured efficiency with the input voltage 24V,36V,and 48V and variable output power ($T_{on} = 10\mu s$).

operating condition of SC converter ($V_{in} = 36V$ and $I_o = 6A$) with the PI controller, the proposed VFCCC controlled SC converter takes about 15.9% of response time. What's more, with the proposed control method, the current ripple of SC converter at the transient time point is less than the PI controlled SC converter.

As shown in Fig.12,the load current and the input voltage are kept stable, the external perturbation is injected into the reference current (the reference current is adjusted from 3-6A or from 6-3A, respectively).It can be seen from Fig.12, the worst-case transient setting time of the VFCCC controlled SC converter is 0.9ms at the condition $V_{in} = 24V$ and I_{ref} step-down 6-3A. While, with the PI control method, the worst-case transient setting time is 4.5mS. As a result, for the VFCCC method, the setting time is 20% that with the conventional PI controller. It can be seen from the experimental results, the proposed control method-controlled SC converter presents the stable operation performance. The advantages of using the proposed VFCCC method in achieving a fast-dynamical response speed over a wide range of operating conditions is demonstrated. The analysis of proposed control method is verified. What's more, the experimental results match very well with the theory analysis.

C. EFFICIENCY

The efficiency of the proposed method controlled SC converter is shown in Fig.13 and Fig.14.The efficiency data is achieved with the constant on time 5us and 10us, respectively. In combination with the proposed control method, the tested

SC converter works under different power levels by adjusting the reference current. In the limited range of SC converter in this paper, the peak efficiency is 97.41% at 3W with the input voltage 36V and the constant on time 5us as shown in Fig.13. With the increasing load current, the efficiency will decrease. It is caused by the higher switching loss and higher input current ripple. The energy losses including the switching loss and the parasitic loss of the circuit. By optimizing the topology of SC converter and utilizing the wide-band gap devices, the efficiency of the proposed SC converter could be further improved in the future work.

The comparison with prior art is shown in Table 2. With the proposed control method, the SC converter-based LED driver provides the good performance such as the high efficiency, high power density and fast-dynamical response speed with the simple topology.

V. CONCLUSIONS AND DISCUSSIONS

This paper proposes a VFCCC method for SC converter-based automotive LED driver. Compared with the inductor-based DC-DC converter used for LED driver, the SC converter could provide higher power density, lower price, and simpler topology. In combination with the proposed control method, the external disturbance of SC converter could be rejected by adjusting switching frequency with the constant on time. It provides fast-dynamical response speed with good regulation. The dimming of LEDs could be changed by just adjusting the reference current. The accuracy and feasibility of proposed controller are demonstrated by the experimental

results. This control method is a general control method. It could be used for different power levels and different topologies of SC converters. It could facilitate the application of SC converter-based automotive LED drivers, especially for the LEDs applications of electric vehicle.

REFERENCES

- [1] Y. Wang, J. Alonso, and X. Ruan, "A review of LED drivers and related technologies," *IEEE Trans. Ind. Electron.*, vol. 64, no. 7, pp. 5754–5765, Jul. 2017.
- [2] H.-T. Chen, S.-C. Tan, and S. Y. Hui, "Nonlinear dimming and correlated color temperature control of bicolor white LED systems," *IEEE Trans. Power Electron.*, vol. 30, no. 12, pp. 6934–6947, Dec. 2015.
- [3] H.-T. Chen, D.-Y. Lin, S.-C. Tan, and S. S. Y. Hui, "Chromatic, photometric and thermal modeling of LED systems with nonidentical LED devices," *IEEE Trans. Power Electron.*, vol. 29, no. 12, pp. 6636–6647, Dec. 2014.
- [4] Y. C. Chung, K. M. Lee, H. J. Choe, C. H. Sung, and B. Kang, "Low-cost drive circuit for AC-direct LED lamps," *IEEE Trans. Power Electron.*, vol. 30, no. 10, pp. 5776–5782, Oct. 2015.
- [5] S. Moon, G.-B. Koo, and W.-G. Moon, "A new control method of interleaved single-stage flyback AC–DC converter for outdoor LED lighting systems," *IEEE Trans. Power Electron.*, vol. 28, no. 8, pp. 4051–4062, Aug. 2013.
- [6] M. D. Seeman, S. R. Sanders, and J. M. Rabaey, "An ultra-low-power power management IC for energy-scavenged wireless sensor nodes," in *Proc. IEEE Power Electron. Spec. Conf.*, pp. 925–931, Jun. 2008.
- [7] Y.-C. Li, "A novel control scheme of quasi-resonant valley-switching for high-power-factor AC-to-DC LED drivers," *IEEE Trans. Ind. Electron.*, vol. 62, no. 8, pp. 4787–4794, Aug. 2015.
- [8] H.-T. Chen, W. C. H. Choy, and S. Y. Hui, "Characterization, modeling, and analysis of organic light-emitting diodes with different structures," *IEEE Trans. Power Electron.*, vol. 31, no. 1, pp. 581–592, Jan. 2016.
- [9] J. Choi, H.-S. Han, and K. Lee, "A current-sourced LED driver compatible with fluorescent lamp ballasts," *IEEE Trans. Power Electron.*, vol. 30, no. 8, pp. 4455–4466, Aug. 2015.
- [10] P. S. Almeida, H. A. C. Braga, M. A. D. Costa, and J. M. Alonso, "Offline soft-switched LED driver based on an integrated bridgeless boost-asymmetrical half-bridge converter," *IEEE Trans. Ind. Appl.*, vol. 51, no. 1, pp. 761–769, Jan./Feb. 2015.
- [11] X. Ruan, B. Wang, K. Yao, and S. Wang, "Optimum injected current harmonics to minimize peak-to-average ratio of LED current for electrolytic capacitor-less AC–DC drivers," *IEEE Trans. Power Electron.*, vol. 26, no. 7, pp. 1820–1825, Jul. 2011.
- [12] Q. Luo, S. Zhi, C. Zou, B. Zhao, and L. Zhou, "Analysis and design of a multi-channel constant current light-emitting diode driver based on high-frequency AC bus," *IET Power Electron.*, vol. 6, no. 9, pp. 1803–1811, Nov. 2013.
- [13] M. Arias, D. G. Lamar, J. Sebastian, D. Balocco, and A. A. Diallo, "High-efficiency LED driver without electrolytic capacitor for street lighting," *IEEE Trans. Ind. Appl.*, vol. 49, no. 1, pp. 127–137, Jan./Feb. 2013.
- [14] S. K. Ng, K. H. Loo, Y. M. Lai, and C. K. Tse, "Color control system for RGB LED with application to light sources suffering from prolonged aging," *IEEE Trans. Ind. Electron.*, vol. 61, no. 4, pp. 1788–1798, Apr. 2014.
- [15] K. Modempalli and L. Parsa, "A scalable N-color LED driver using single inductor multiple current output topology," *IEEE Trans. Power Electron.*, vol. 31, no. 5, pp. 3773–3783, May 2016.
- [16] X. Wu, C. Hu, J. Zhang, and Z. Qian, "Analysis and design considerations of LLC resonant multioutput DC/DC LED driver with charge balancing and exchanging of secondary series resonant capacitors," *IEEE Trans. Power Electron.*, vol. 30, no. 2, pp. 780–789, Feb. 2015.
- [17] Y. Qin, S. Li, and S. Y. Hui, "Topology-transition control for wide-input-voltage-range efficiency improvement and fast current regulation in automotive LED applications," *IEEE Trans. Ind. Electron.*, vol. 64, no. 7, pp. 5883–5893, Jul. 2017.
- [18] Y. Wang, S. Gao, Y. Guan, J. Huang, D. G. Xu, and W. Wang, "A single-stage LED driver based on double LLC resonant tanks for automobile headlight with digital control," *IEEE Trans. Transport. Electrification*, vol. 2, no. 3, pp. 357–368, Sep. 2016.
- [19] L. Corradini and G. Spiazzi, "A high-frequency digitally controlled LED driver for automotive applications with fast dimming capabilities," *IEEE Trans. Power Electron.*, vol. 29, no. 12, pp. 6648–6659, Dec. 2014.
- [20] S. Mukherjee, A. Sepahvand, and D. Maksimović, "High-frequency LC³L resonant DC-DC converter for automotive LED driver applications," in *Proc. IEEE Appl. Power Electron. Conf. Expo.*, Mar. 2018, pp. 797–802.
- [21] K.-I. Hwu and W.-Z. Jiang, "Input-current-ripple-free two-channel LED driver," *IEEE Trans. Ind. Electron.*, vol. 64, no. 7, pp. 5865–5874, Jul. 2017.
- [22] C. S. Wong, K. H. Loo, H. H.-C. Iu, Y. M. Lai, M. H. L. Chow, and C. K. Tse, "Independent control of multicolor-multistring LED lighting systems with fully switched-capacitor-controlled LCC resonant network," *IEEE Trans. Power Electron.*, vol. 33, no. 5, pp. 4293–4305, May 2018.
- [23] D. Kilani, M. Alhawari, B. Mohammad, H. Saleh, and M. Ismail, "An efficient switched-capacitor DC-DC buck converter for self-powered wearable electronics," *IEEE Trans. Circuits Syst. I, Reg. Papers*, vol. 63, no. 10, pp. 1557–1566, Oct. 2016.
- [24] T. Tong, S. K. Lee, X. Zhang, D. Brooks, and G.-Y. Wei, "A fully integrated reconfigurable switched-capacitor DC-DC converter with four stacked output channels for voltage stacking applications," *IEEE J. Solid-State Circuits*, vol. 51, no. 9, pp. 2142–2152, Sep. 2016.
- [25] R. Jain et al., "A 0.45–1 V fully-integrated distributed switched capacitor DC-DC converter with high density MIM capacitor in 22 nm tri-gate CMOS," *IEEE J. Solid-State Circuits*, vol. 49, no. 4, pp. 917–927, Feb. 2014.
- [26] D. F. Cortez, G. Waltrich, J. Fraigneaud, H. Miranda, and I. Barbi, "DC–DC converter for dual-voltage automotive systems based on bidirectional hybrid switched-capacitor architectures," *IEEE Trans. Ind. Electron.*, vol. 62, no. 5, pp. 3296–3304, May 2015.
- [27] P. E. Bolzan, V. L. Rosa, G. Denardin, and R. N. do Prado, "Switched capacitor with dimming feature to feed LED tubular lamp," in *Proc. IEEE Int. Conf. Ind. Technol. (ICIT)*, Lyon, France, Feb. 2018, pp. 571–574.
- [28] C. Le, D. L. Gerber, M. Kline, S. R. Sanders, and P. R. Kinget, "Reconfigurable hybrid-switched-capacitor-resonant LED driver for multiple mains voltages," *IEEE J. Emerg. Sel. Topics Power Electron.*, vol. 6, no. 4, pp. 1871–1883, Dec. 2018.
- [29] M. Martins, M. S. Perdigão, A. S. Mendes, R. A. Pinto, and J. M. Alonso, "Dimmable LED driver with variable inductor based on a resonant switched-capacitor topology," in *Proc. Energy Convers. Congr. Expo.*, 2015, pp. 5329–5336.
- [30] M. Martins, M. S. Perdigão, A. M. S. Mendes, R. A. Pinto, and J. M. Alonso, "Analysis, design, and experimentation of a dimmable resonant-switched-capacitor LED driver with variable inductor control," *IEEE Trans. Power Electron.*, vol. 32, no. 4, pp. 3051–3062, Apr. 2016.
- [31] J. C. Castellanos, M. Turhan, and E. Cantatore, "A 93.3% peak-efficiency self-resonant hybrid-switched-capacitor LED driver in 0.18- μm CMOS technology," *IEEE J. Solid-State Circuits*, vol. 53, no. 7, pp. 1924–1935, Jul. 2018.
- [32] W. Feng and F. G. Shi, "A new switched-capacitor frequency modulated driver for light emitting diodes," *Rev. Sci. Instrum.*, vol. 78, no. 11, pp. 114701–1–114701–4, Nov. 2007.
- [33] E. E. dos Santos Filho, P. H. A. Miranda, E. M. Sá, and F. L. M. Antunes, "A LED driver with switched capacitor," *IEEE Trans. Ind. Appl.*, vol. 50, no. 5, pp. 3046–3054, Sep. 2014.
- [34] R. P. Coutinho, K. C. A. de Souza, F. L. M. Antunes, and E. Sa, "Three-phase resonant switched capacitor LED driver with low flicker," *IEEE Trans. Ind. Electron.*, vol. 64, no. 7, pp. 5828–5837, Jul. 2017.
- [35] Y. Qu, W. Shu, and J. S. Chang, "A low-EMI, high-reliability PWM-based dual-phase LED driver for automotive lighting," *IEEE J. Emerg. Sel. Topics Power Electron.*, vol. 6, no. 3, pp. 1179–1189, Mar. 2018.
- [36] B. Wu, L. Yang, X. Zhang, K. M. Smedley, and G.-P. Li, "Modeling and analysis of variable frequency one-cycle control on high-power switched-capacitor converters," *IEEE Trans. Power Electron.*, vol. 33, no. 6, pp. 5465–5475, Jun. 2018.
- [37] L. Yang, B. Wu, X. Tong, K. M. Smedley, and G.-P. Li, "Dynamic capacitor ampere-second balance transient calculation modeling method for switched-capacitor converters," *IEEE Trans. Power Electron.*, vol. 33, no. 10, pp. 8916–8926, Oct. 2018.
- [38] K. M. Smedley and S. Čuk, "One-cycle control of switching converters," *IEEE Trans. Power Electron.*, vol. 10, no. 6, pp. 625–633, Nov. 1995.



LEI YANG (S'15–M'17) was born in Henan, China, in 1986. He received the B.S. degree in electric and information engineering from Information Engineering University, Zhengzhou, China, in 2011, the M.S. degree in signal and information processing (SIP), and the Ph.D. degree in electrical engineering from Northwestern Polytechnical University, Xi'an, China, in 2014 and 2017, respectively.

From 2014 to 2016, he was a Visiting Student with the University of California at Irvine, Irvine, CA, USA. He is currently an Assistant Professor with the Xi'an University of Technology. His research interests include nonlinear control, switched-capacitor (SC) converter, dc–dc converter, power source of electrical vehicle, wireless power and data transfer systems, and renewable energy integration.



WENQIAN YU (S'17) was born in Shaanxi, China, in 1995. She received the B.S. degree in electrical engineering from the Xi'an University of Technology, Xi'an, China, in 2017, where she is currently pursuing the master's degree.

Her research interests include nonlinear control, active power filter (APF), switched-capacitor (SC) converter, and dc–dc converter.



JIAYANG ZHANG (S'17) was born in Shaanxi, China, in 1994. He is currently pursuing the master's degree in electrical engineering with the Xi'an University of Technology.

His research interests include bidirectional-dc/dc converter, nonlinear control method, switched-capacitor (SC) converter, dc–dc converter, power source of electrical vehicle, and ac/dc hybrid microgrid.

...